Proc. NIPR Symp. Antarct. Meteorites, 1, 14-37, 1988

PETROCHEMICAL STUDY OF THE YAMATO-691 ENSTATITE CHONDRITE (E3) II: DESCRIPTIONS AND MINERAL COMPOSITIONS OF UNUSUAL SILICATE-INCLUSIONS

Yukio IKEDA

Department of Earth Sciences, Faculty of Science, Ibaraki University, 1-1, Bunkyo 2-chome, Mito 310

Abstract: The Yamato (Y)-691 chondrite includes unusual silicate-inclusions besides chondrules. An inclusion containing high CaO and Al_2O_3 contents and other opaque massive inclusions containing high FeO content are similar in bulk chemical compositions to fine-grained CAI's and amoeboid olivine inclusions in carbonaceous chondrites, respectively. They are concluded to be melted fine-grained CAI's and melted amoeboid olivine inclusions. Most unusual inclusions containing high FeO content were originally high-temperature condensates under oxidized conditions and followed by melting events. After the consolidation, they were brought into extremely reduced conditions, where they accreted with magnesian chondrules on a parent body of the Y-691 enstatite chondrite.

1. Introduction

The Yamato (Y)-691 chondrite consists of unusual silicate-inclusions, chondrules, opaque-mineral nodules, mineral fragments and matrix. The bulk chemical compositions of unusual silicate-inclusions and chondrules in Y-691 were presented in the proceeding paper (IKEDA, 1988a), and this paper deals with detailed description of unusual silicate-inclusions and chemical compositions of the constituent minerals. The following papers (IKEDA, 1988b, c) will treat chondrules and opaque-mineral nodules in Y-691. Unusual silicate-inclusions in Y-691 are mainly opaque massive objects which are opaque and massive under the microscope, showing various outlines. Sometimes it is observed under the microscope that they contain small amounts of silicate crystals set in the opaque massive objects. In addition to these inclusions, some glassy objects which contain high contents of CaO and Al_2O_3 occur in Y-691, and they are also presented as unusual silicate-inclusions in this paper.

The unusual silicate-inclusions are quite different in bulk chemical compositions from most chondrules (IKEDA, 1988a); particularly opaque massive inclusions contain high FeO contents in comparison to most chondrules. Recently, ubiquitous occurrences of FeO-bearing objects in many enstatite chondrites were reported (RAMBALDI *et al.*, 1983, 1984; PRINZ *et al.*, 1984, 1985; NAGAHARA, 1985; BISCHOFF *et al.*, 1985; LUSBY *et al.*, 1987), although the origin of the FeO-bearing objects in enstatite chondrites is not yet clarified. In this paper detailed description of FeO-bearing inclusions in Y-691 and their origin will be discussed together with glassy inclusions containing high CaO and Al_2O_3.

2. Analytical Method

Chemical compositions of silicates and oxides were obtained using a fixed focussed beam of an electron-probe micro-analyzer (EPMA; JEOL Superprobe 733, accelerating voltage 15 kV, sample current 3 to 5 nA). However, aggregates consisting of fine-grained Mg-silicates and Fe-metal (and/or troilite), which are defined to be decomposed-olivine in this paper and were produced from ferroan olivine by reduction, were analyzed using a scanning focussed or fixed defocussed beam of EPMA. For the case of analyses using a scanning focussed beam, standard materials were also measured using the same scanning focussed beam. Correction method of BENCE and ALBEE (1968) was used. Troilite and Fe-metal were corrected by standard ZAF method. The mineral compositions obtained are tabulated in the Appendix.

3. Unusual Silicate-Inclusions

3.1. No. 172

A glassy inclusion, No. 172 (Fig. 1), includes many small laths of crystals set in a glassy groundmass. The size of laths is a few microns in width and 10 to 15 microns in length. They are fassaitic pyroxene, and seem to be quenched crystals crystallizing from a silicate melt during a rapid cooling event.

Chemical compositions of the pyroxene and groundmass of the inclusion are given in the Appendix. As the pyroxene laths are narrow, the chemical compositions obtained correspond to a mixture of the lath and the surrounding groundmass; for example, the high alkali content of the pyroxene (Appendix, $Na_2O=0.93$ wt%) may come from the surrounding groundmass. Although the groundmass is heterogeneous, the chemical compositions seem to be similar to that of the pyroxene laths, except for the high alkali content of the former. The Mg/(Mg+Fe) atomic ratios (hereafter, mg values) of the pyroxene and glass are nearly the same with the range of 0.974–0.998. The bulk

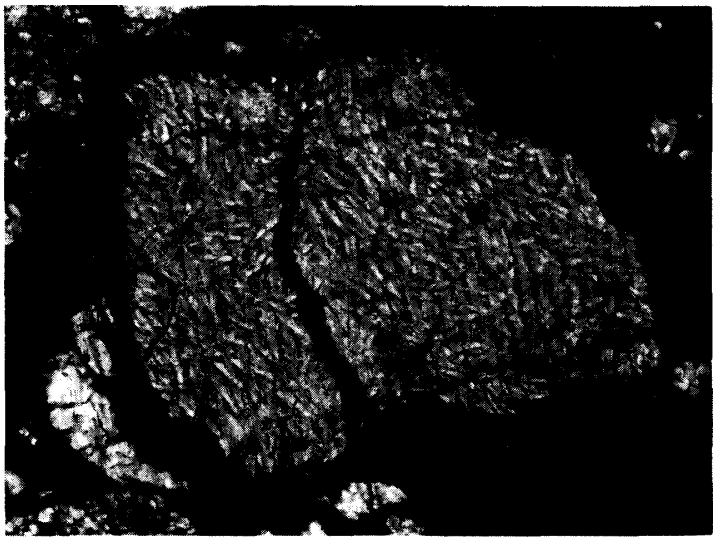

Fig. 1. Photomicrograph (transmitted light) of inclusion No. 172. Width of figure: 570 microns.

composition of the inclusion is similar to that of fine-grained CAI's occurring in carbonaceous chondrites except for the low FeO content of the former (IKEDA, 1988a), suggesting that it was produced originally as a fine-grained CAI and it was melted by a heating event and cooled rapidly, resulting in the quenched texture.

3.2. No. 167

Inclusion No. 167 is ellipsoidal, with a size of 400×500 microns (Fig. 2), and consists of pyroxene laths with interstitial glass. The width and length of the laths are about 10 and 50 microns, respectively. Small amounts of opaque phases occur.

The pyroxenes are low-Ca pyroxenes (Appendix) including about 3 wt% of Al_2O_3. The mg values are about 0.96–0.97. The groundmass glass is very heterogeneous, and the chemical compositions correspond to those of mixtures of olivine, pyroxene, and plagioclase in various proportions. The mg of the groundmass ranges from 0.94 to 0.96. It is suggested that the inclusion originally consisted of olivine, pyroxene and plagioclase, and it was melted by a heating event and cooled so soon as the melt was not homogenized, resulting in the quenched texture.

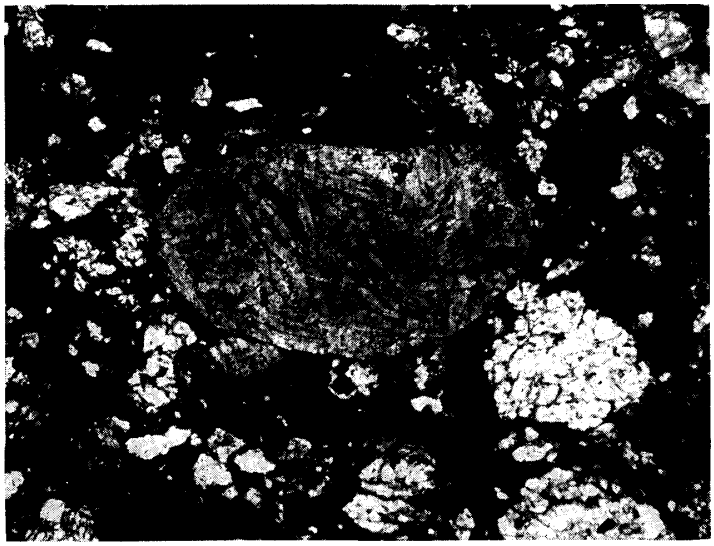

Fig. 2. Photomicrograph (transmitted light) of inclusion No. 167. Width of figure: 1150 microns.

3.3. No. 152

An unusual silicate-inclusion, No. 152, is opaque and massive under the microscope (Figs. 3 and 4). However, backscattered electron images reveal that it consists mainly of decomposed-olivine grains with small amounts of fassaite, aluminous augite, subcalcic augite, pigeonite, calcic to intermediate plagioclase, albite, spinel, sulfide, and metal. The overall texture of the inclusion is that large grains of decomposed-olivine are packed closely and the interstices are filled with minor phases such as pyroxenes. A decomposed-olivine grain is an aggregate consisting of Mg-silicates (enstatite and/or forsterite) and Fe-metal with small amounts of relic ferroan olivine and troilite, showing striped patterns (Figs. 5 and 6). Each band of the striped patterns is less than a few

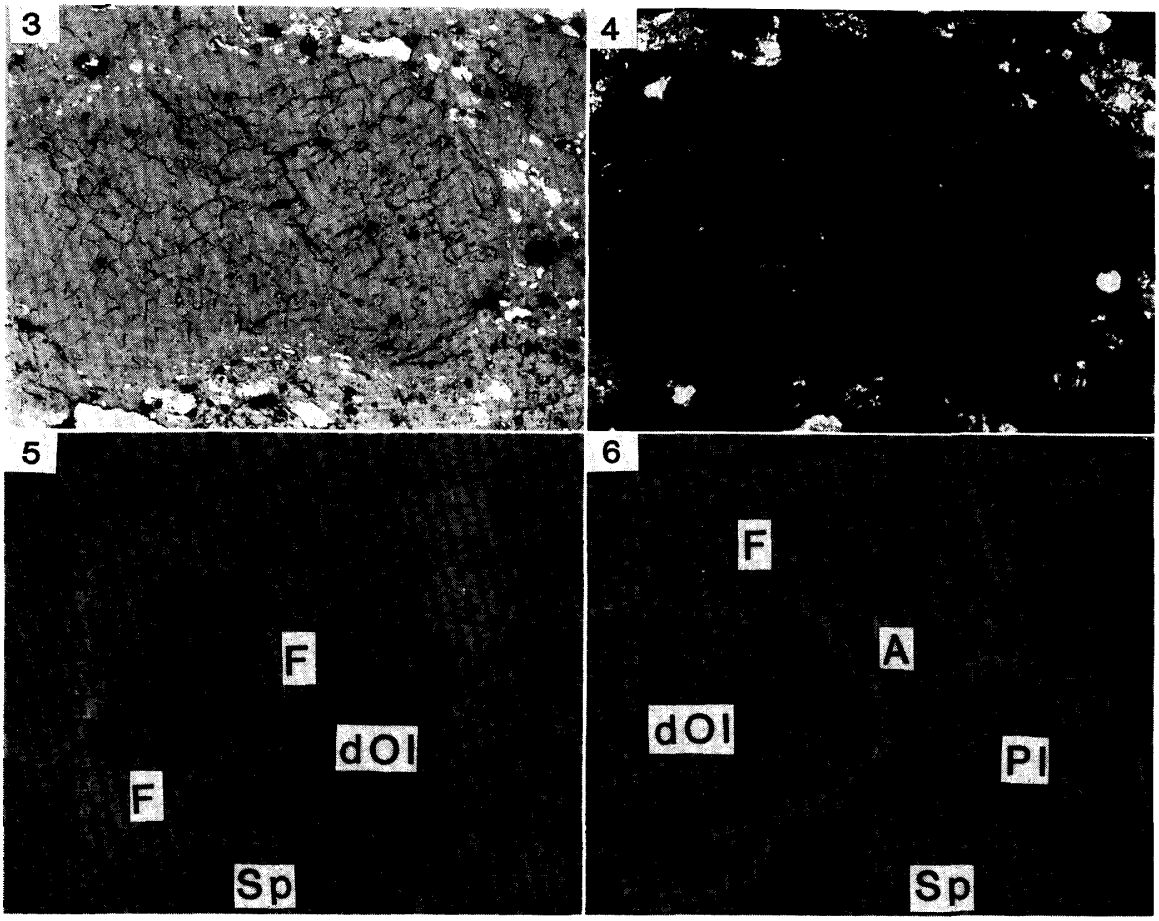

Figs. 3 to 6. Inclusion No. 152. Figures 3 and 4 are photomicrographs in reflected light and transmitted light, respectively, and widths are 1150 microns. Figures 5 and 6 are back-scattered electron (BSE) images, and widths are 110 and 63 microns, respectively. F, Sp, dOl, A, and Pl are fassaite, spinel, decomposed-olivine, augite, and plagioclase, respectively. Note the occurrence of augite and plagioclase as pseudomorph after fassaite in Fig. 6.

microns in width. The orientation of striped patterns of decomposed-olivine grains is nearly the same throughout the inclusion. The bulk chemical compositions of decomposed-olivine grains correspond to that of ferroan olivine with mg=about 0.86 (Appendix), and they seem to have been produced from ferroan olivines by reduction and/or sulfurization.

The reaction of olivine-decomposition to produce Mg-silicates is as follows on the assumption that SiO_2 components were supplied from a surrounding nebular gas;

$$\underset{\text{Ol}}{Mg_{2-x}Fe_xSiO_4} + \underset{\text{Gas}}{xH_2} + \underset{\text{Gas}}{(1-x)SiO_2} \longrightarrow \underset{\text{En}}{(2-x)MgSiO_3} + \underset{\text{Met}}{xFe} + \underset{\text{Gas}}{xH_2O}, \quad (1)$$

and if the supply of the SiO_2 component was not enough, the reaction is;

$$\underset{\text{Ol}}{Mg_{2-x}Fe_xSiO_4} + \underset{\text{Gas}}{xH_2} \longrightarrow \underset{\text{Fo}}{(1-x)Mg_2SiO_4} + \underset{\text{En}}{xMgSiO_3} + \underset{\text{Met}}{xFe} + \underset{\text{Gas}}{xH_2O}, \quad (2)$$

where x is about 0.3 for inclusion No. 152. Reactions (1) and (2) can take place at the same time in an inclusion, depending upon the diffusivity of the SiO_2 component in the inclusion. The bulk compositions of most decomposed-olivine grains show that the atomic ratios of (Mg+Fe)/Si are nearly 2 (Appendix), suggesting that the main reaction to decompose ferroan olivine was reaction (2), for inclusion No. 152.

In addition to enstatite occurring in decomposed-olivine grains, four kinds of pyroxenes occur in the interstices between the decomposed-olivine grains. They are fassaite, aluminous augite, subcalcic augite, and pigeonite. Fassaites occur as euhedral or subhedral forms between decomposed-olivine grains. On the other hand, aluminous augite, subcalcic augite and pigeonite occur as pseudomorphs after fassaite grains, together with plagioclase. A compositional gap is observed between fassaite and aluminous augite, although aluminous augite seems to be continuous in composition to pigeonite via subcalcic augite (Figs. 19 to 21). These occurrences of the pyroxenes suggests that aluminous augite to pigeonite were originally fassaites which later changed, in the inclusion, to the assemblages of (Aug to Pig+calcic Pl) by the following reactions;

$$\underset{\text{Fassaite Solid Solution}}{n\mathrm{Ca(Mg,\,Fe)Si_2O_6}} + \mathrm{CaAlAlSiO_6} + \underset{\text{Gas}}{\mathrm{SiO_2}} \longrightarrow \underset{\text{Aug}}{n\mathrm{Ca(Mg,\,Fe)Si_2O_6}} + \underset{\text{An}}{\mathrm{CaAl_2Si_2O_8}}, \quad (3)$$

where n is about 3 for the case of inclusion No. 152, and

$$\underset{\text{Aug}}{\mathrm{Ca(Mg,\,Fe)Si_2O_6}} + \underset{\text{Gas}}{m\mathrm{SiO_2}} + \underset{\text{Ol}}{m\mathrm{(Mg,\,Fe)_2SiO_4}} \longrightarrow \underset{\text{Pig}}{\mathrm{Ca(Mg,\,Fe)_{1+2m}Si_{2+2m}O_{6+6m}}}, \quad (4)$$

where m is about 3 for the case of inclusion No. 152. At the same time as or after reaction (3), the augite components changed to pigeonite by reaction (4) with introduction of SiO_2 from a nebular gas. The mg values of fassaite, aluminous augite, subcalcic augite, and pigeonite in the inclusion are 0.83–0.85, 0.73–0.79, 0.74–0.78, and 0.72–0.80, respectively. The latter three values are similar to each other and more ferroan than the fassaite. These low mg values mean that reactions (3) and (4) took place under oxidized conditions.

Plagioclase always occurs associated with aluminous augite, subcalcic augite or pigeonite. Their compositions range from $An_{64}Ab_{35}$ to $An_{88}Ab_{12}$. The anorthite component may be formed by reaction (3) from the Ca-Tschermak molecule of fassaite. Formation of the albite component needs addition of Na_2O from a nebular gas, and the possible reactions are as follows:

$$\underset{\text{Ca-Tsch}}{\mathrm{CaAl_2SiO_6}} + \underset{\text{Gas}}{\mathrm{Na_2O}} + \underset{\text{Gas}}{6.5\mathrm{SiO_2}} + \underset{\text{Ol}}{0.5\mathrm{(Mg,\,Fe)_2SiO_4}} \longrightarrow \underset{\text{Ab}}{2\mathrm{NaAlSi_3O_8}} + \underset{\text{Aug}}{\mathrm{Ca(Mg,\,Fe)Si_2O_6}}, \quad (5)$$

or

$$\underset{\text{An}}{\mathrm{CaAl_2Si_2O_8}} + \underset{\text{Gas}}{\mathrm{Na_2O}} + \underset{\text{Gas}}{5.5\mathrm{SiO_2}} + \underset{\text{Ol}}{0.5\mathrm{(Mg,\,Fe)_2SiO_4}} \longrightarrow \underset{\text{Ab}}{2\mathrm{NaAlSi_3O_8}} + \underset{\text{Aug}}{\mathrm{Ca(Mg,\,Fe)Si_2O_6}}. \quad (6)$$

These reactions may have taken place at the same time as reactions (3) and (4), resulting in calcic to intermediate plagioclases in inclusion No. 152. In addition to the calcic to intermediate plagioclase, a small amount of sodic plagioclase is observed in the outermost rim of the inclusion; its composition is about $An_{1-2}Ab_{94}$.

Spinel occurs as subhedral forms between decomposed-olivine grains (Figs. 5 and 6), associated with pyroxene or plagioclase. The spinel is poor in TiO_2 (about 0.3–0.4 wt%) and rich in Cr_2O_3 (about 23–28 wt%). The FeO content of most spinel is low (0.4–0.5 wt%) with some exceptions of FeO-bearing spinel up to 2.2 wt% FeO. The mg values of most spinel are extremely high (about 0.99).

Fe-metal occurs as small rods along the lineations of the striped patterns of decomposed-olivines (Figs. 5 and 6). The length and width of the rods are less than several microns and one micron, respectively. On the other hand, troilite occurs mainly as relatively large grains, up to a few tens of microns across, in interstices between decomposed-olivine grains. Chemical composition of troilite is 36.2 wt% S, 1.1 wt% Cr, and 59.9 wt% Fe. The Cr content is high and similar to those of troilites occurring in the opaque-mineral nodules of Y-691 (IKEDA, 1988c).

The bulk composition of inclusion No. 152 is similar to that of amoeboid olivine inclusions occurring in carbonaceous chondrites (IKEDA, 1988a). This suggests that inclusion No. 152 was originally produced as a high-temperature condensate under oxidized conditions, which consisted mainly of ferroan olivine, fassaite and probably spinel. However, the texture of the inclusion is quite different from those of amoeboid olivine inclusions. Therefore, the high-temperature condensates might have experienced a melting event, and ferroan olivine firstly crystallized from the melt. After the crystallization of the olivine, the residual melt was enriched in CaO and Al_2O_3, and ferroan fassaite and ferroan and chromian spinel crystallized to fill the interstices between the large ferroan olivine grains. After the consolidation of the inclusion, the fassaite reacted with the surrounding oxidized nebular gas to produce augite to pigeonite and calcic to intermediate plagioclase in the inclusion. Finally, it was brought into extremely reduced conditions, where ferroan olivine reacted with the reduced gas by reactions (1) and/or (2) to decompose the ferroan olivine into the aggregates of Mg-silicates (enstatite and/or forsterite) and Fe-metal (and/or troilite). The ferroan spinel may have changed to magnesian spinel by diffusional exchange of Mg and Fe under the extremely reduced condition, whereas the exchange did not take place in the ferroan pyroxenes. Albitic plagioclase may have formed in the peripheral part by the introduction of alkalies from the surrounding reduced gas.

3.4. No. 300

Inclusion No. 300 shows a spherical outline with a diameter of about 500 microns. The texture is strange (Fig. 7), although pseudomorphs of barred-Ol-Px texture are weakly recognized in some parts of the inclusion (Fig. 8), where olivine has been decomposed to aggregates of Mg-silicates and Fe-metal (and/or troilite). The degrees of decomposition differ in the inclusion; some portions consist of coarse-grained enstatite and Fe-metal although other portions show striped patterns consisting of narrow bands of Mg-silicates (enstatite and/or forsterite) and Fe-metal (Fig. 8). The bulk compositions of decomposed-olivine grains showing striped patterns correspond to that of ferroan

olivines with mg values ranging from 0.86 to 0.92. The decomposition may have taken place by reactions (1) and/or (2). However, the coarse-grained enstatite seems to have formed from ferroan olivine by reaction (1). A pyroxene rim imperfectly fringes the inclusion, the width of rim being a few microns (Fig. 7).

In addition to enstatite, FeO-bearing pyroxene occurs within the inclusion. It is bronzite and the mg values are 0.86–0.89 in contrast with the values of 0.992–0.995 for enstatite. The pyroxene rim surrounding the inclusion is similar in chemical composition to the bronzite occurring within the inclusion, the mg being 0.87–0.89.

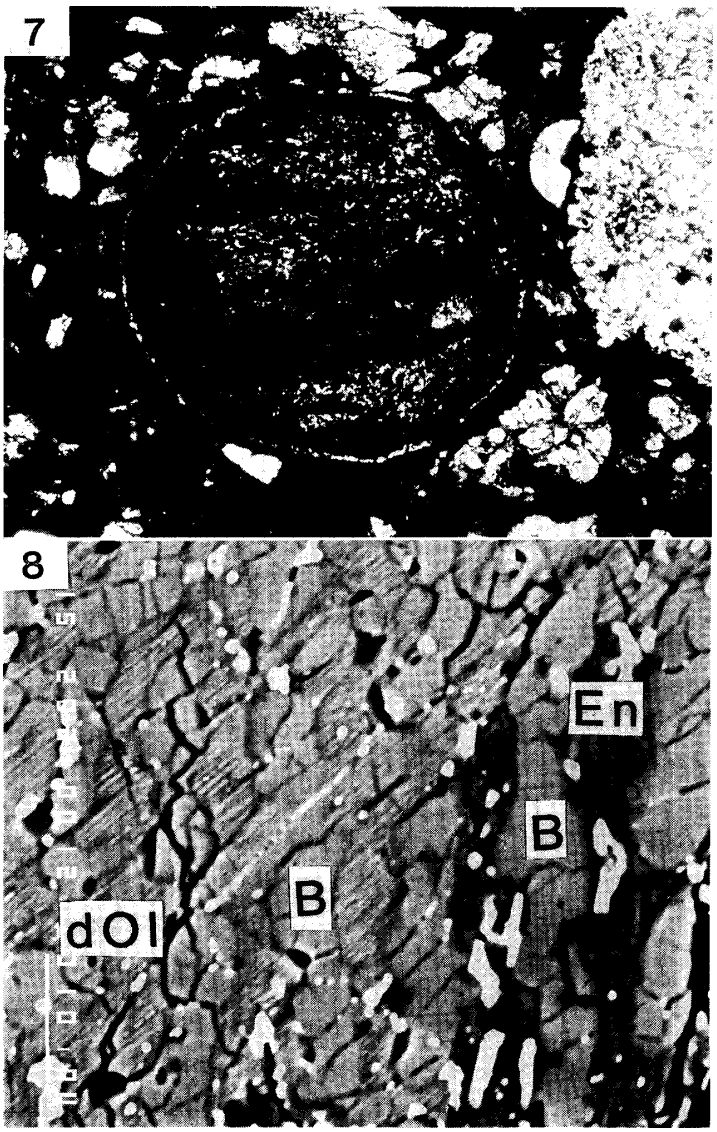

Figs. 7 and 8. Photomicrograph (7, transmitted light) and BSE image (8) of inclusion No. 300. Widths of Figs. 7 and 8 are 1150 and 63 microns, respectively. En, B, and dOl are enstatite (dark), bronzite (gray bars), and decomposed-olivine (striped pattern), respectively. Minerals in bright are Fe-metal and troilite. Note the occurrence of enstatite as pseudomorph after ferroan olivine bars.

Inclusion No. 300 is considered to have originally consisted of ferroan olivine and bronzite, surrounded by a narrow rim of bronzite. The inclusion was brought into extremely reduced conditions, the ferroan olivine reacting with the reduced gas to form enstatite, and probably forsterite, within the inclusion.

3.5. No. 303

An unusual silicate-inclusion, No. 303, is opaque and massive under the microscope, has a rectangular outline, and is 750×230 microns (Fig. 9). It consists mainly of decomposed-olivine and plagioclase with small amounts of spinel, enstatite, nepheline, sulfide and Fe-metal. Decomposed-olivine and plagioclase show a barred-Ol-Pl texture, the bar width ranging from a few to several tens of microns (Fig. 10). The decomposed-olivine comprises fine-grained Mg-silicates (enstatite and/or forsterite), Fe-metal, troilite and relic ferroan olivine. The Mg-silicates seem to form by reactions (1) and/or (2). Large enstatite (Fig. 10), up to a few tens of microns across, occurs surrounded by Fe-metal. The enstatite occurs as pseudomorphs after olivine-bars, suggesting that it was produced by reaction (1).

Spinel occurs as rounded grains (Fig. 10), about 10 microns across, associated with plagioclase. The spinel contains small amounts of FeO, about 2 to 3 wt%, the mg values being about 0.93 to 0.95. The atomic ratios of Cr/Al of the spinel are lower than those in inclusion No. 152. Plagioclase is calcic in composition, ranging from $An_{80}Ab_{20}$ to $An_{70}Ab_{30}$. It is replaced partly by nepheline. A few large nepheline grains occur in the peripheral parts of the inclusion, and the composition is shown in the Appendix. The reaction to form nepheline from calcic plagioclase is as follows;

$$\underset{\text{An}}{CaSi_2Al_2O_8} + \underset{\text{Gas}}{Na_2O} \longrightarrow \underset{\text{Ne}}{2NaSiAlO_4} + CaO, \qquad (7)$$

and the CaO of the right hand side has been lost from the inclusion during the reaction, probably forming Ca-bearing phases such as high-Ca pyroxene outside the inclusion. On the other hand, albite occurs at the rim of the inclusion, fringing the large nepheline grains. The albite may have formed by the following reaction from nepheline;

$$\underset{\text{Ne}}{NaSiAlO_4} + \underset{\text{Gas}}{2SiO_2} \longrightarrow \underset{\text{Ab}}{NaSi_3AlO_8}. \qquad (8)$$

Inclusion No. 303 is considered to have originally consisted of calcic plagioclase and ferroan olivine with small amounts of ferroan spinel, showing a barred-Ol-Pl texture. Then the calcic plagioclase reacted with a SiO_2-depleted nebular gas to form nepheline with introduction of Na_2O from the gas by reaction (7). Because nepheline is a common mineral in FeO-bearing fine-grained CAI's in carbonaceous chondrites, reaction (7) may have taken place in an oxidized condition similar to that of fine-grained CAI's. After that, the inclusion was brought into extremely reduced conditions, where the ferroan olivine decomposed by reactions (1) and/or (2), and albite formed at the rim of the inclusion by reaction (8).

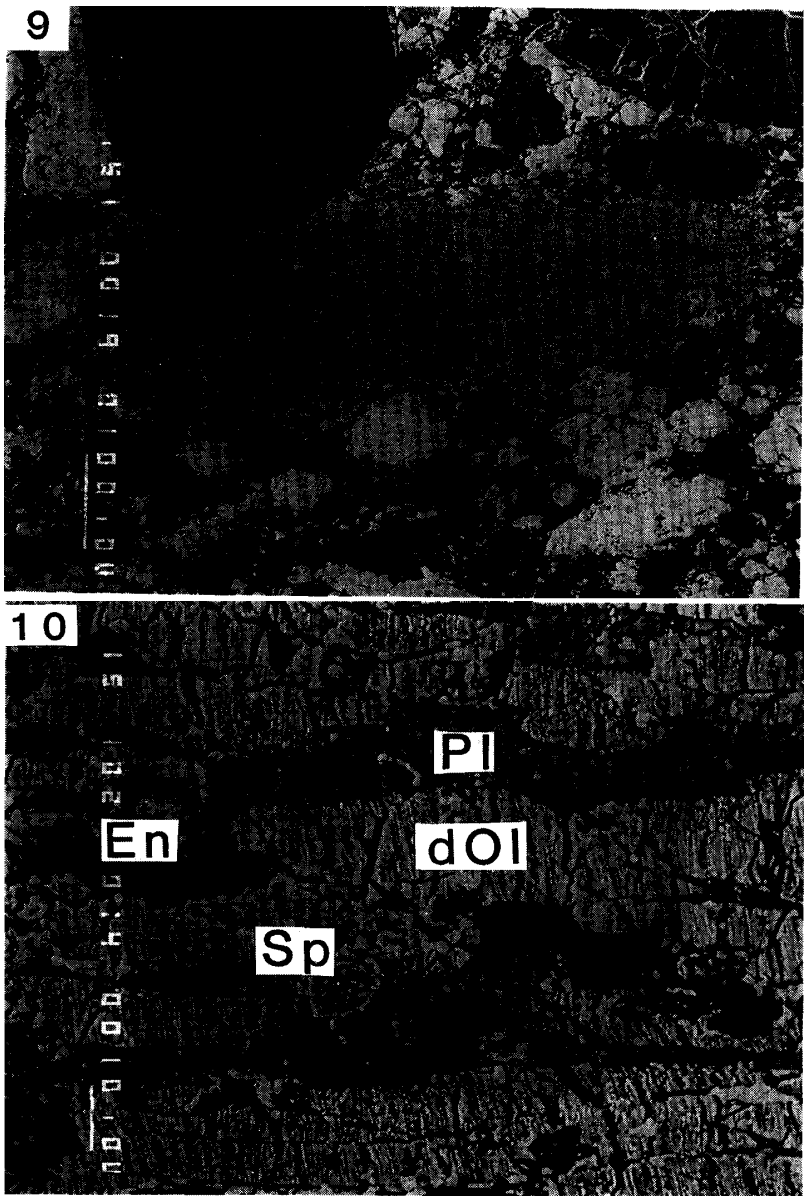

Figs. 9 and 10. BSE images of inclusion No. 303. Widths of Figs. 9 and 10 are 840 and 124 microns, respectively. En, Pl, dOl, and Sp are enstatite (dark), plagioclase (gray), decomposed-olivine (striped), and spinel (a rounded grain, about 10 microns across), respectively. Minerals in bright are Fe-metal and troilite.

3.6. No. 302

Inclusion No. 302 is opaque and massive under the microscope and the size is 350× 650 microns (Fig. 11). It consists mainly of decomposed-olivine, fassaite, and groundmass. The back-scattered electron images show a barred-Ol-Px texture, the width being about several microns for decomposed-olivine and a few microns for fassaite (Fig. 12). The decomposed-olivine consists of fine-grained Mg-silicates and Fe-metal (and/or troilite) although fassaite does not seem to decompose in the inclusion.

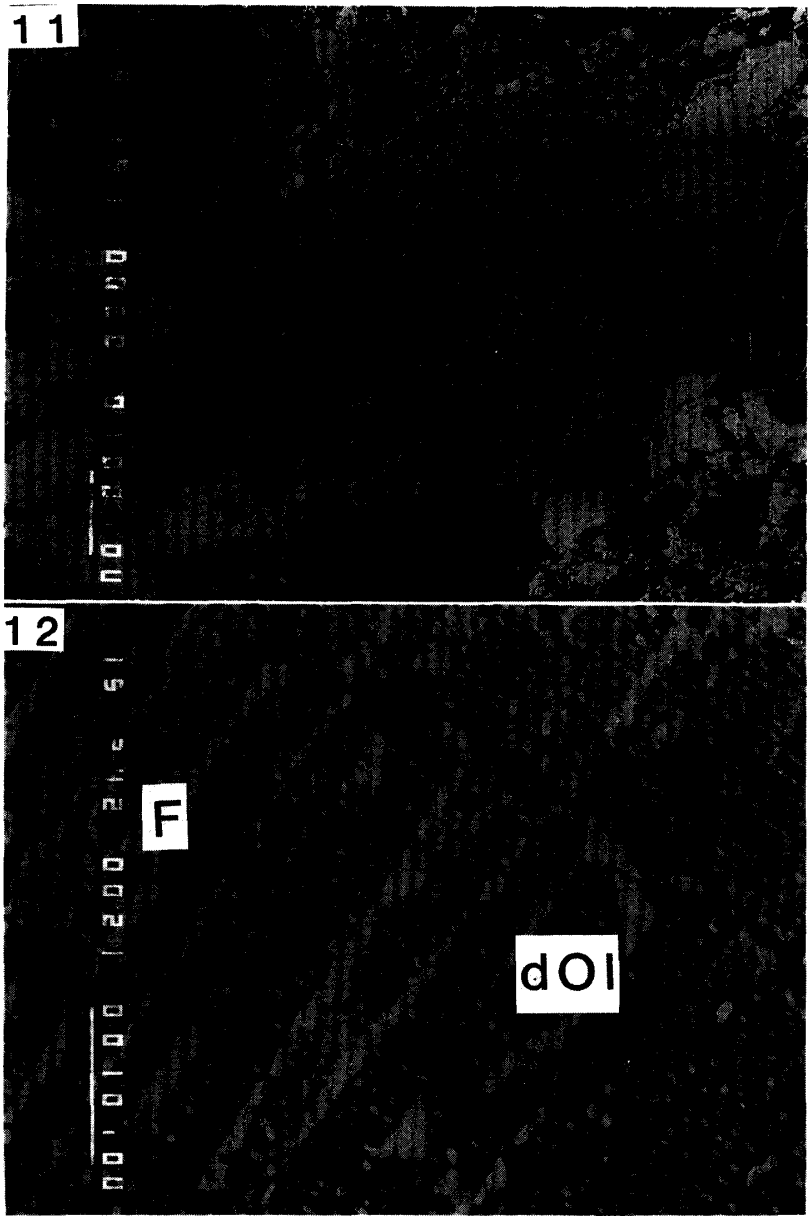

Figs. 11 and 12. BSE images of inclusion No. 302. Widths are 840 and 53 microns, respectively. F and dOl are fassaite (gray bars) and decomposed-olivine (striped), respectively. Bright dots are Fe-metal and troilite.

3.7. No. 114

Inclusion No. 114 is an opaque massive object under the microscope and shows a round shape with a diameter of 340 microns (Fig. 13). It consists mainly of decomposed-olivine, bronzite, enstatite, Fe-metal and troilite, showing a barred-Ol-Px texture. The widths of bars are several microns (Fig. 14). The degree of decomposition of ferroan olivine seems to be various in the inclusion; some portions of olivine pseudomorphs consist of coarse-grained enstatite and Fe-metal, although other portions are decomposed-olivine which are aggregates of fine-grained Mg-silicates, Fe-metal (and/or troilite) and probably relic ferroan olivine.

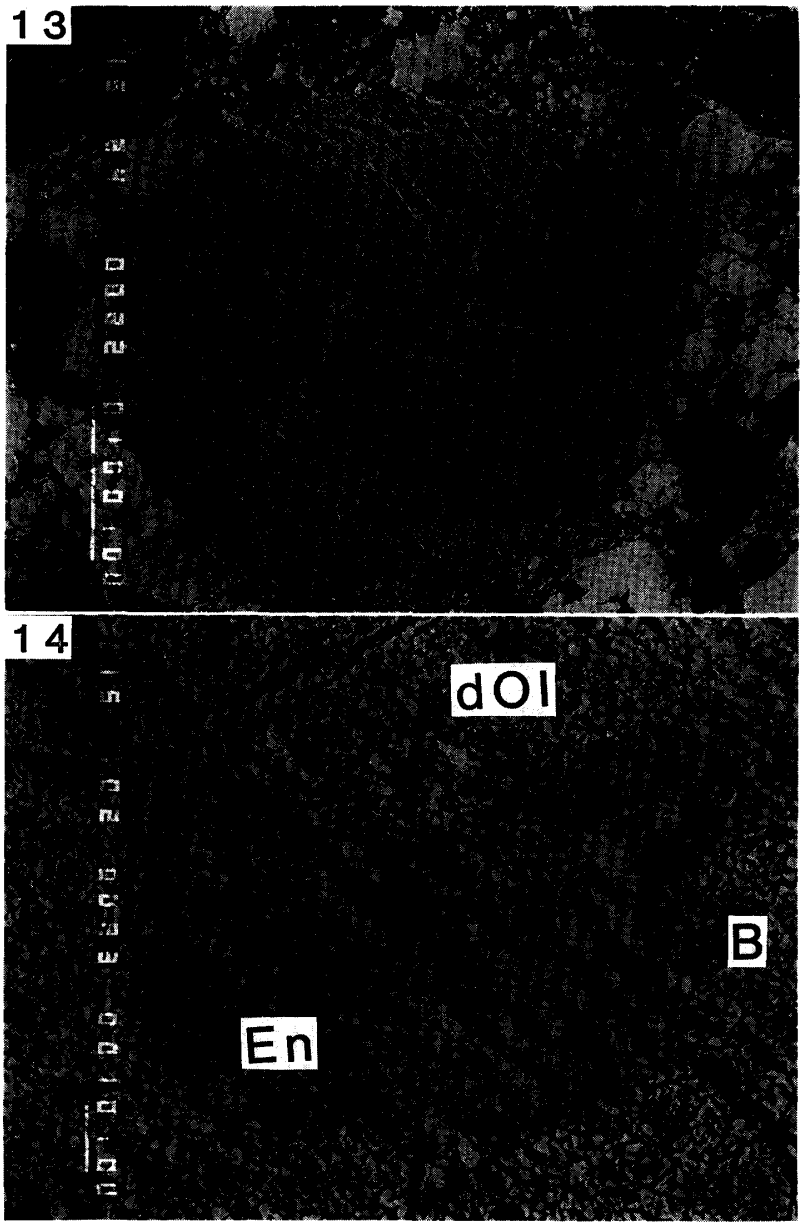

Figs. 13 and 14. BSE images of inclusion No. 114. Widths are 530 and 117 microns, respectively. Symbols are the same as those in Fig. 8. Minerals in bright are Fe-metal and troilite.

Large opaque minerals, up to ten microns across, occur in the inclusion (Fig. 14). Although they are mostly troilite, a few grains are Fe-metal. The chemical composition of Fe-metal is 89.5 wt%Fe, 0.5 wt%Co, 4.0 wt%Ni, 2.0 wt%Si and 0.1 wt%Cr, and is similar in composition to those occurring in opaque-mineral nodules of Y-691 (IKEDA, 1988c).

The inclusion is considered to have originally consisted of ferroan olivine with mg values less than 0.84–0.88 and bronzite with mg=0.82, showing a barred-Ol-Px texture. It was brought into an extremely reduced condition and reactions (1) and (2) took place to decompose the ferroan olivine.

3.8. No. 237

Inclusion No. 237 is an opaque massive object with several bars of pyroxene under the microscope (Fig. 15). It consists mainly of decomposed-olivine, diopside, pigeonite and plagioclase, showing a barred-Ol-Px-Pl texture (Fig. 16). The decomposed-olivine bars are 10 to 20 microns in width, consisting of fine-grained Mg-silicates, Fe-metal and relic ferroan olivine. Pyroxenes are diopside and pigeonite, showing euhedral forms. The mg values are about 0.95 for decomposed-olivine, 0.92–0.94 for pigeonite and 0.93–0.94 for diopside. Plagioclase occurs as an interstice-filling phase (Fig. 16), suggesting that it was the last phase which crystallized from the residual melt. The composition is $An_{62-75}Ab_{36-24}$.

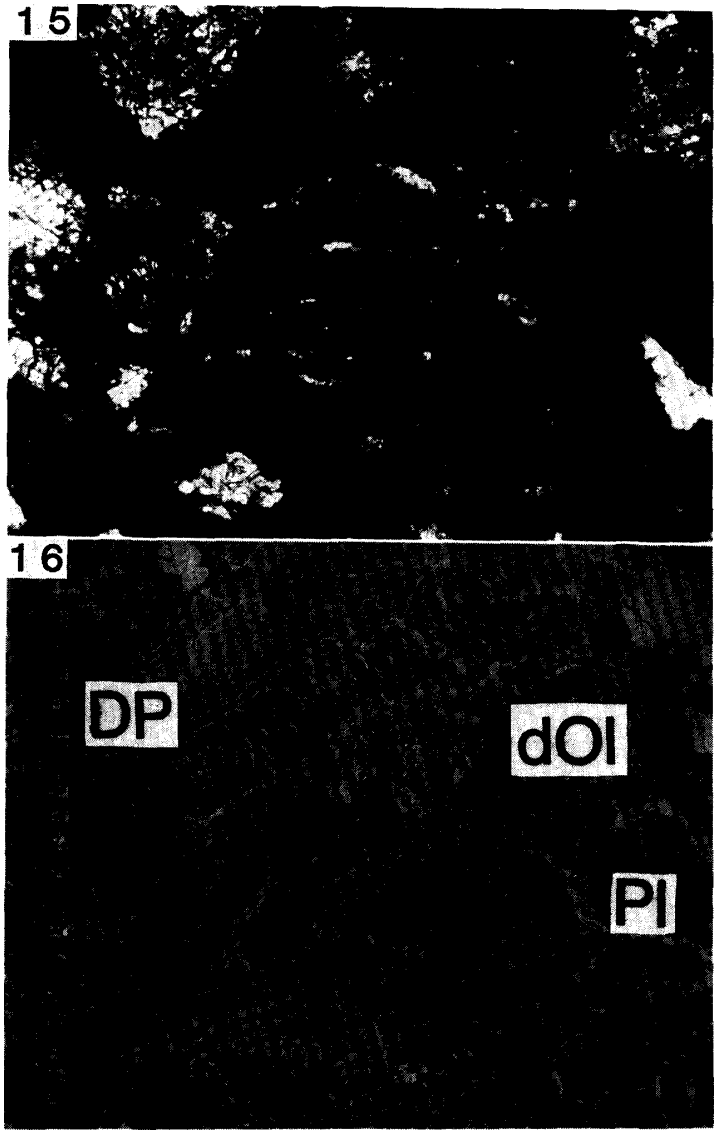

Figs. 15 and 16. Photomicrograph (15, transmitted light) and BSE image (16) of inclusion No. 237. Widths of Figs. 15 and 16 are 570 and 160 microns, respectively. DP, Pl and dOl are diopside and pigeonite, plagioclase and decomposed-olivine, respectively.

3.9. No. 304

Inclusion No. 304 shows a strange texture under the microscope (Fig. 17). BSE images (Fig. 18) reveal that the texture is striped patterns with layers of about a few micron width. The layers consist of bronzite and Mg-silicates with small rounded grains of Fe-metal or troilite. The mg values of bronzite are about 0.86. The chemical composition of Mg-silicates is not obtained because the layers are too narrow to be analyzed. The Mg-silicates may be produced by reactions (1) and/or (2) under reduced conditions without any reaction for the coexisting bronzite.

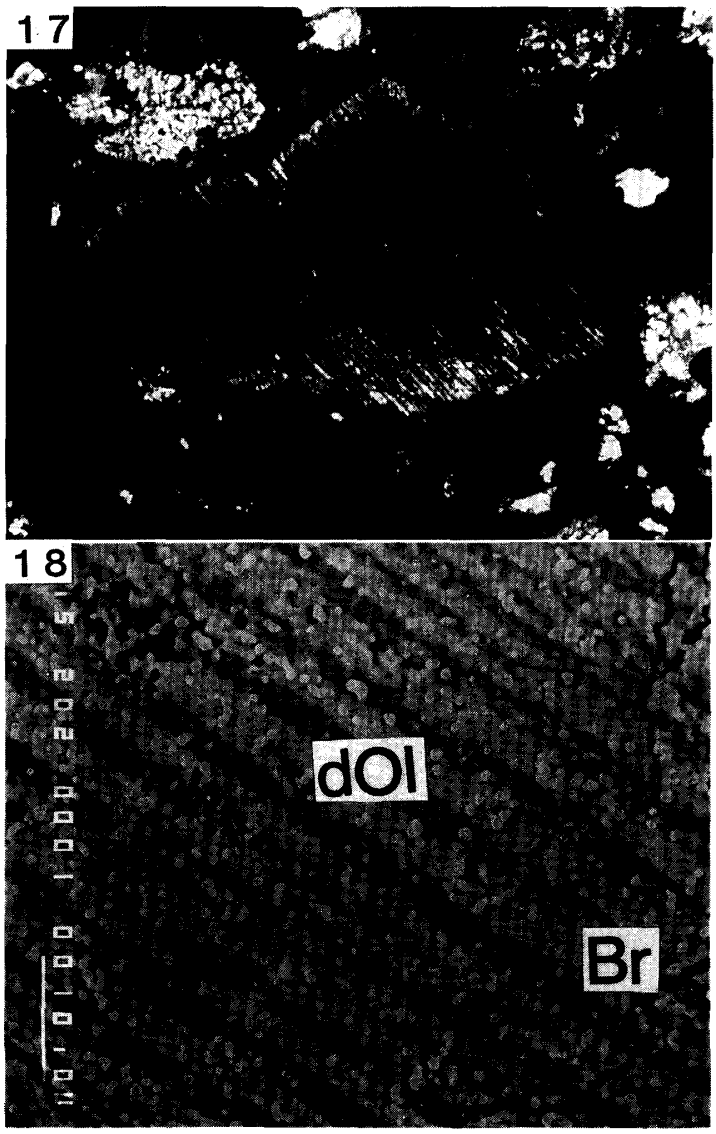

Figs. 17 and 18. Photomicrograph (17, transmitted light) and BSE image (18) of inclusions No. 304. Widths of Figs. 17 and 18 are 570 and 62 microns, respectively. Br (gray bars) and dOl (dark bars) are bronzite and Mg-silicates, reapectively. Bright dots are Fe-metal or troilite.

4. Mineralogy

4.1. *Fassaite*

Fassaites are included in unusual silicate-inclusions, Nos. 172, 152 and 302, and their chemical compositions are plotted in Figs. 19 to 21. The fassaite in No. 172 is

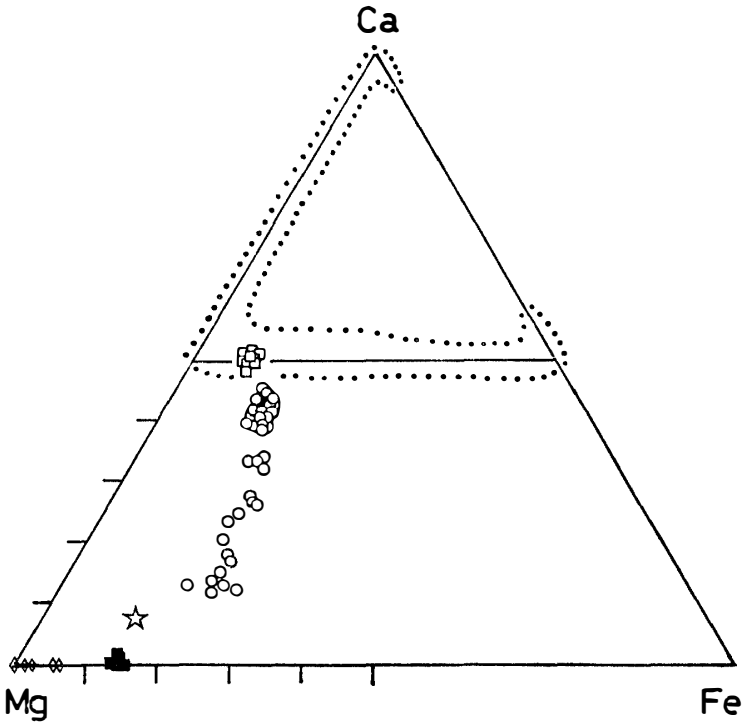

Fig. 19. Ca-Mg-Fe plot of pyroxene, spinel and olivine in atomic ratio.

(a) inclusion No. 152; fassaite (open squares), augite-subcalcic augite-pigeonite (open circles), spinel (open diamonds), decomposed-olivine (solid squares) and bulk composition of the inclusion (star). Compositional range of pyroxene and pyroxenoid in CAI's of carbonaceous chondrites (GROSSMAN, 1975; ALLEN et al., 1978) is shown by dotted line.

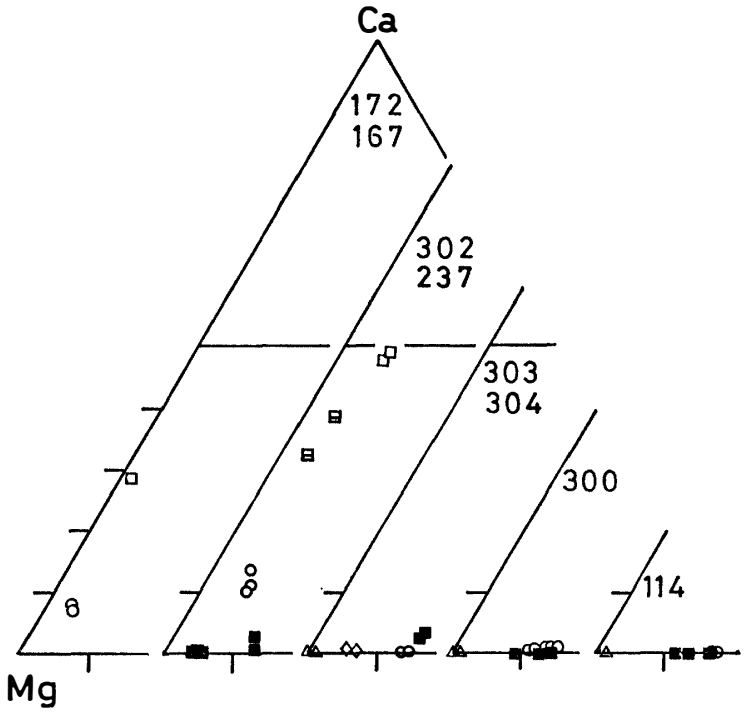

(b) inclusions Nos. 172, 167, 302, 237, 303, 304, 300 and 114. Fassaitic pyroxene (open squares), diopside (No. 237, open squares with horizontal bar), low-Ca pyroxene (open circles), secondary enstatite (open triangles), spinel (open diamonds) and decomposed-olivine (solid squares) are shown.

extremely enriched in Al_2O_3, but the TiO_2 content is not so high in comparison to fassaites occurring in CAI's of carbonaceous chondrites (GROSSMAN, 1975; ALLEN *et al.*, 1978; DOMINIK *et al.*, 1978; MEEKER *et al.*, 1983; MACDOUGALL *et al.*, 1981; KORNACKI and WOOD, 1985; ARMSTRONG *et al.*, 1985; WARK and LOVERING, 1977, 1982a, b). The CaO content of No. 172 is very low (Fig. 19b), and it may be a metastable phase.

On the other hand, the fassaites in Nos. 152 and 302 include high FeO contents and the mg values are nearly the same as those of decomposed-olivine, suggesting that the ferroan fassaites were nearly in equilibrium with the ferroan olivine prior to decomposition by reaction (3).

In comparison to fassaites occurring in CAI's of carbonaceous chondrites, the fassaites in Nos. 152 and 302 are low in Ti/Al. The low ratios are similar to those in fine-grained CAI's of the ALH-77003 carbonaceous chondrite (IKEDA, 1982), whereas fassaites of the latter are magnesian and comprise small amounts of FeO less than 0.5 wt%.

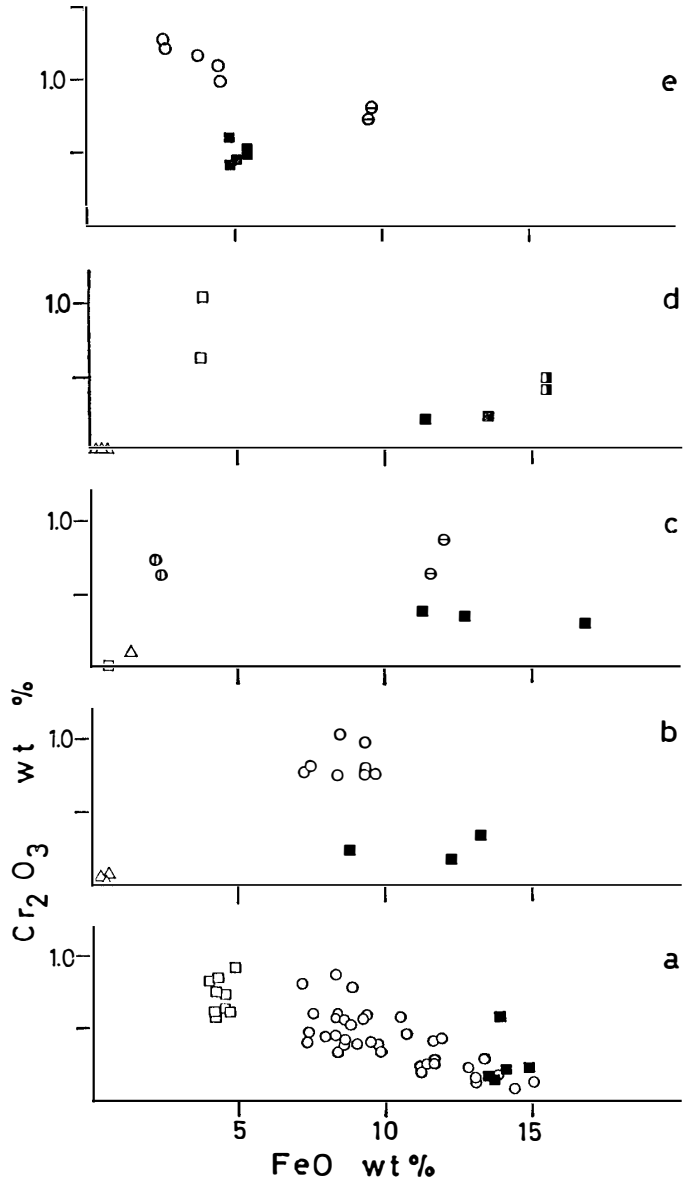

Fig. 20. FeO-Cr_2O_3 plot of pyroxene and olivine in wt%.
(a) inclusion No. 152, fassaite (open squares), augite-subcalcic augite-pigeonite (open circles) and decomposed-olivine (solid squares).
(b) inclusion No. 300, bronzite (open circles), secondary enstatite (open triangles) and decomposed-olivine (solid squares).
(c) low-Ca pyroxene of No. 167 (circles with vertical bar); fassaitic pyroxene of No. 172 (open square); bronzite (circles with horizontal bar), secondary enstatite (open triangle) and decomposed-olivine (solid squares) in inclusion No. 114.
(d) fassaite (open squares) and decomposed-olivine (solid squares) in inclusion No. 302; secondary enstatite (open triangles) and decomposed-olivine (half-solid squares) in inclusion No. 303.
(e) diopside and pigeonite (open circles) and decomposed-olivine (solid squares) in inclusion No. 237; bronzite (open circles with horizontal bar) in inclusion No. 304.

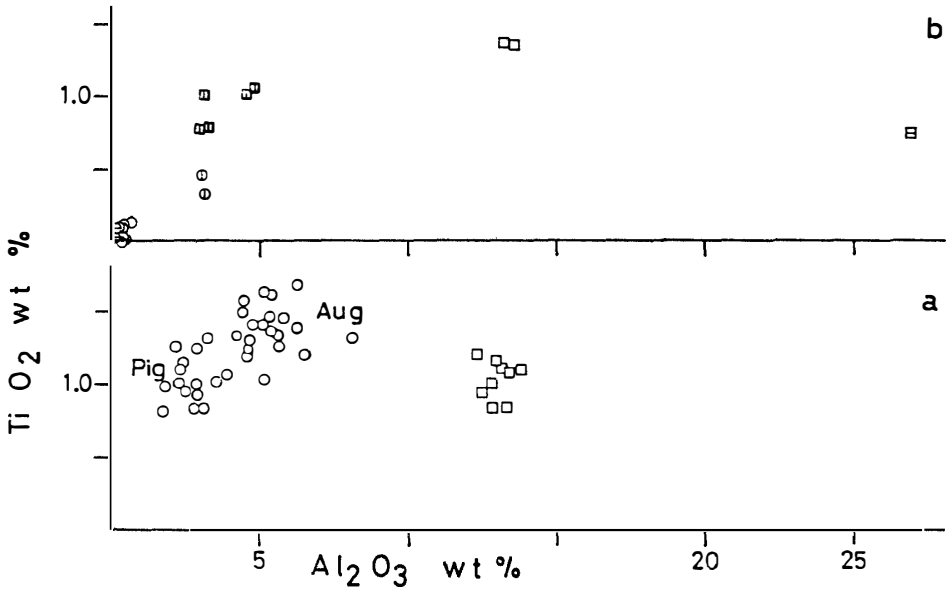

Fig. 21. *Al_2O_3-TiO_2 plot of pyroxenes. (a) inclusion No. 152, fassaite (open square) and augite-subcalcic augite-pigeonite (open circles). (b) No. 172 fassaite (square with horizontal bar), No. 302 fassaite (open squares), No. 167 low-Ca pyroxene (circle with vertical bar), No. 300 bronzite (open circle), No. 114 bronzite (circle with horizontal bar), and No. 237 diopside and pigeonite (open squares with vertical bar).*

4.2. Augite, diopside and pigeonite

Augite and pigeonite occur in inclusion No. 152, and diopside and pigeonite are observed in inclusion No. 237. As already stated, the former are considered to be produced from fassaite in subsolidus conditions, and subcalcic augite in No. 152 may be a metastable phase. On the other hand, diopside and pigeonite in No. 237 are primary phases which crystallized from the residual melt. The TiO_2 and Al_2O_3 contents of augite, diopside and pigeonite in Nos. 152 and 237 are similar to each other (Fig. 21), although the Cr_2O_3 contents of the pyroxene are higher for No. 237 than those for No. 152.

4.3. Bronzite and enstatite

Bronzite occurs in inclusions Nos. 300, 304 and 114, being a primary phase which crystallized from the melts. The bronzite is extremely depleted in refractory lithophiles such as CaO, TiO_2 and Al_2O_3, although it includes moderate amounts of Cr_2O_3 ranging from 0.5 to 1.0 wt%. This suggests that the precursor materials of the inclusions were products under oxidized conditions, which were already depleted in high-temperature condensates.

Enstatite in inclusion No. 167 is a primary phase which crystallized from a melt. On the other hand, most enstatite in other inclusions occurs as a secondary phase which was produced from ferroan olivine in subsolidus conditions. Although the primary enstatite contains variable amounts of CaO, Al_2O_3, Cr_2O_3, FeO and TiO_2 (Figs. 19 to 21), the secondary ones are nearly free from those components.

4.4. Spinel

Compositions of spinels in inclusions Nos. 152 and 303 are plotted in Fig. 22. In comparison to spinels occurring in CAI's of carbonaceous chondrites, the spinels in Nos. 152 and 303 are extremely rich in Cr_2O_3. On the other hand, they are extremely poor in FeO in comparison to most spinels occurring in ordinary chondrites.

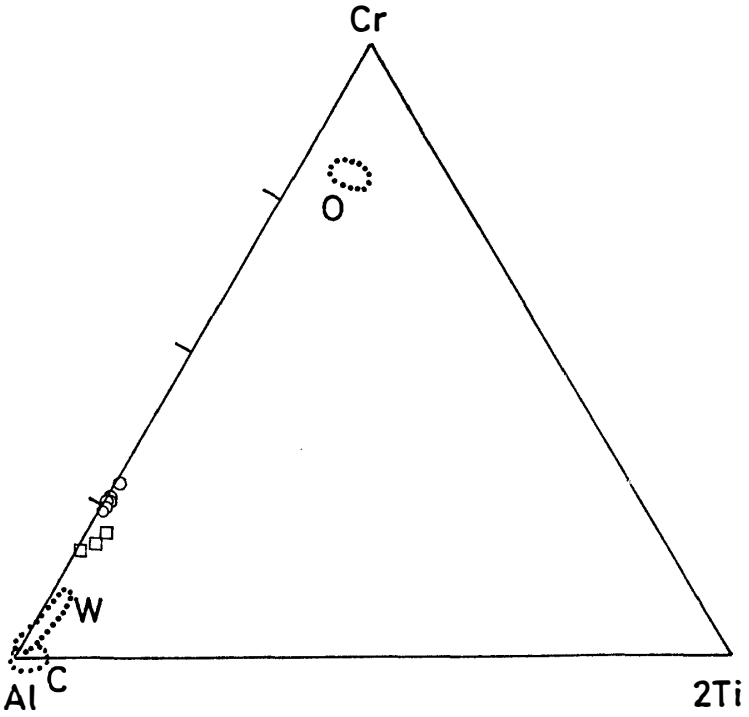

Fig. 22. Al-Cr-2Ti plot of spinels in atomic ratio. Spinels in No. 152 (open circles) and in No. 303 (open squares) are shown with reference of compositional ranges of spinels in CAI's (C; GROSSMAN, 1975), Willy inclusion (W; ARMSTRONG et al., 1985), and equilibrated ordinary chondrites (O; IKEDA, unpublished data).

Originally the spinels in Nos. 152 and 303 were probably in equilibrium with ferroan olivine and must have included abundant FeO. The diffusion coefficients of Mg and Fe are larger for spinels than for olivine (LEHMAN, 1983) and probably than for pyroxenes. Therefore, diffusional exchange of Mg and Fe can take place more easily for spinel than for olivine and pyroxenes. This supports the conclusion already stated in the foregoing section that FeO-poor and Cr_2O_3-bearing spinels in Nos. 152 and 303 were produced from FeO-rich and Cr_2O_3-bearing spinels by diffusional exchange under extremely reduced conditions.

4.5. Plagioclase

Calcic to intermediate plagioclases are included in Nos. 152, 237 and 303. The plagioclase in No. 152 occurs as a secondary phase which was produced by reactions (3), (5) and/or (6). The calcic to intermediate plagioclase in Nos. 303 and 237 occurs as bars or as an interstice-filling phase, showing a barred-Ol-Pl or barred-Ol-Px-Pl texture.

The plagioclase was a primary phase which crystallized after the crystallization of ferroan olivine and/or pyroxene under rapid-cooling conditions.

5. Discussion

Ubiquitous occurrences of FeO-bearing objects in other enstatite chondrites were reported (RAMBALDI *et al.*, 1983, 1984; PRINZ *et al.*, 1984, 1985; LUSBY *et al.*, 1987). NAGAHARA (1985) reported the occurrence of decomposed-olivine as mineral fragments set in the matrix of Y-691. The ubiquitous occurrences of FeO-bearing objects have been explained by multi-stage processes of formation (NAGAHARA, 1985; PRINZ *et al.*, 1985). LUSBY *et al.* (1987) presented detailed explanations for the origin of FeO-bearing objects, including crystallization of FeO-rich melts, modification by nebula or planetary reduction along cracks, reduction of chondrule melts, collisions of partly molten chondrules, and so on. In addition to FeO-bearing objects, BISCHOFF *et al.* (1985) found refractory inclusions and Al-rich chondrules in some enstatite chondrites and discussed the origin.

The formation of FeO-bearing inclusions described in this paper includes the following stages in this order; (A) Condensation of FeO-bearing materials under highly-oxidized conditions and formation of the precursors of the unusual silicate-inclusions. (B) Melting of the precursors, followed by crystallization and/or quenching. (C) Reactions of the inclusions with the surrounding oxidized nebular gases. (D) Translation of the inclusions from oxidized gases into reduced nebular gases. (E) Reactions of the inclusions with the reduced nebular gases. (F) Accretion onto the parent body of Y-691. (G) Metamorphism in the parent body.

Stage (A) is suggested by the fact that the bulk compositions of inclusions Nos. 152, 302 and 303 are similar to those of amoeboid olivine inclusions in carbonaceous chondrites (IKEDA, 1988a). IKEDA (1982) concluded that the original materials of amoeboid olivine inclusions in carbonaceous chondrites consisted mainly of olivine with minor amounts of fassaite and spinel, and suggested the possibility that ferroan olivine condensed directly from an oxidized nebular gas prior to the condensation of alkalies. If so, the original materials of Nos. 152, 302 and 303 in Y-691 may have consisted of aggregates of ferroan olivine, fassaite, and spinel, which condensed directly from an oxidized nebular gas at high temperatures. The FeO-bearing inclusions, Nos. 300, 304 and 114, are depleted in refractory lithophile elements (IKEDA, 1988a) and condensation of the precursors of the inclusions may have taken place in a relatively-low temperature range, and the precursors may have been already depleted in refractory components.

Stage (B) is necessary to produce the igneous textures of the unusual silicate-inclusions. Barred-Ol-Px (Nos. 300, 114 and 304), barred-Ol-Pl (Nos. 302 and 303) and barred-Ol-Px-Pl (No. 237) textures suggest that the melts cooled rapidly. Stage (C) explains the occurrence of ferroan augite to pigeonite and calcic to intermediate plagioclase in inclusion No. 152 and their formation in solid state by reactions (3) to (6) with oxidized nebular gases. Nepheline in No. 303 may have formed under oxidized conditions, because high FeO needs large amounts of SiO_2 to produce fayalite components, resulting in the condensation of alkalies as nepheline instead of albite in low temperature range.

Stages (D) and (E) are necessary for the occurrence of FeO-bearing inclusions in the reduced chondrite Y-691 and for the decomposition of ferroan olivines into Mg-silicates shown by reactions (1) and (2). However, the ferroan pyroxenes did not decompose during the period of decomposition of ferroan olivines, suggesting that the reactions may have taken place at low temperature and had a short duration.

The occurrence of albite in inclusions Nos. 152 and 303 indicates that albite formed after the formation of calcic to intermediate plagioclase or nepheline. As albite and free-silica occur commonly in opaque-mineral nodules and magnesian chondrules of Y-691, albite in the inclusions is considered to have formed in stages (E) to (G).

It is difficult to explain the genesis of the FeO-free inclusion No. 172 by the same processes as for the FeO-bearing inclusions because it contains a large amount of alkalies. The bulk composition of the inclusion is similar to that of fine-grained CAI's in carbonaceous chondrites (IKEDA, 1988a), although fine-grained CAI's contain various and large amounts of FeO. The inclusion can be explained by the following two different hypotheses; (i) The precursor of the inclusion formed at stage (A) as a high-temperature condensate, including FeO and alkalies. During stage (B), reduction of FeO into Fe-metal took place and the Fe metal produced was removed from the melt, resulting in the FeO-free and alkali-bearing composition of the melt, which was finally quenched. (ii) Another hypothesis is that the precursor of No. 172 was a high-temperature condensate from a moderately-oxidized or reduced gas, which was nearly free from ferroan iron and alkalies. With decreasing temperature of the nebular gas, the condensation of alkalies took place prior to the condensation of FeO components, resulting in FeO-free and alkali-bearing composition of the No. 172 precursor. Finally it experienced stage (B), forming a quenched texture. The second hypothesis is preferable because Fe-metal does not occur in the inclusion No. 172.

Acknowledgments

I would like to express my thanks to NIPR for the Y-691 sample preparation and co-operation with the consortium on Y-691. This study has been supported by a Grant in Aid for Scientific Research, from the Ministry of Education, Science and Culture.

References

ALLEN, J.M., GROSSMAN, L., DAVIS, A.M. and HUTCHEON, I.D. (1978): Mineralogy, textures and mode of formation of a hibonite-bearing Allende inclusion. Proc. Lunar Planet. Sci. Conf., 9th, 1209–1233.

ARMSTRONG, J.T., EL GORESY, A. and WASSERBURG, G.J. (1985): Willy: A prize noble Ur-Fremdlinge —Its history and implications for the formation of Fremdlinge and CAI. Geochim. Cosmochim. Acta, **49**, 1001–1022.

BENCE, A.E. and ALBEE, A.L. (1968): Empirical correction factors for the electron microanalysis of silicates and oxides. J. Geol., **76**, 382–403.

BISCHOFF, A., KEIL, K. and STOFFLER, D. (1985): Perovskite-hibonite-spinel-bearing inclusions and Al-rich chondrules and fragments in enstatite chondrites. Chem. Erde, **44**, 97–106.

DOMINIK, B., JESSBERGER, E.K., STAUDACHER, T., NAGEL, K. and EL GORESY, A. (1978): A new type of white inclusions in Allende; Petrology, mineral chemistry, Ar40–Ar39 ages and genetic implications. Proc. Planet. Sci. Conf., 9th, 1249–1266.

EL GORESY, A., ARMSTRONG, J.T. and WASSERBURG, G.J. (1985): Anatomy of an Allende coarse-

grained inclusions. Geochim. Cosmochim. Acta, **49**, 2433–2444.
GROSSMAN, L. (1975): Petrography and mineral chemistry of Ca-rich inclusions in the Allende meteorite. Geochim. Cosmochim. Acta, **39**, 433–454.
IKEDA, Y. (1980): Petrology of Allan Hills-764 chondrite (LL3). Mem. Natl Inst. Polar Res., Spec. Issue, **17**, 50–82.
IKEDA, Y. (1982): Petrology of the ALH-77003 chondrite (C3). Mem. Natl Inst. Polar Res., Spec. Issue, **25**, 34–65.
IKEDA, Y. (1988a): Petrochemical study of the Yamato-691 enstatite chondrite (E3) I; Major element chemical compositions of chondrules and inclusions. Proc. NIPR Symp. Antarct. Meteorites, **1**, 3–13.
IKEDA, Y. (1988b): Petrochemical study of the Yamato-691 enstatite chondrite (E3) III; Descriptions and mineral compositions of chondrules. submitted to Mem. Natl Inst. Polar Res., Ser. G (Meteorite).
IKEDA, Y. (1988c): Petrochemical study of the Yamato-691 enstatite chondrite (E3) IV; Descriptions and mineral chemistry of opaque-mineral nodules. submitted to Mem. Natl Inst. Polar Res., Ser. G (Meteorite).
KORNACKI, A.S. and WOOD, J.A. (1985): Mineral chemistry and origin of spinel-rich inclusions in the Allende CV3 chondrite. Geochim. Cosmochim. Acta, **49**, 1219–1237.
LEHMAN, J. (1983): Diffusion between olivine and spinel; Application to geothermometry. Earth Planet. Sci. Lett., **64**, 123–138.
LUSBY, D., SCOTT, E.R.D. and KEIL, K. (1987): Ubiquitous high-FeO silicates in enstatite chondrites. Proc. Lunar Planet. Sci. Conf., 17th, Pt. 2, E679–E695 (J. Geophys. Res., **92** (B4)).
MACDOUGALL, J.D., KERRIDGE, J.F. and PHINNEY, D. (1981). Refractory ABC. Lunar and Planetary Science XII. Houston, Lunar Planet. Inst., 643–645.
MEEKER, G. P., WASSERBURG, G. J. and ARMSTRONG, J. T. (1983): Replacement textures in CAI and implications regarding planetary metamorphism. Geochim. Cosmochim. Acta, **47**, 707–721.
NAGAHARA, H. (1985): Multi-stage reduction in the primitive enstatite chondrites. Lunar and Planetary Science XVI. Houston, Lunar Planet. Inst., 607–608.
PRINZ, M., NEHRU, C.E., WEISBERG, M.K. and DELANEY, J.S. (1984): Type 3 enstatite chondrites; A newly recognized group of unequilibrated enstatite chondrites (UEC's). Lunar and Planetary Science XV. Houston, Lunar Planet. Inst., 653–654.
PRINZ, M., WEISBERG, M.K., NEHRU, C.E. and DELANEY, J.S. (1985): ALHA81189, a highly unequilibrated enstatite chondrite; Evidence for a multistage history. Meteoritics, **20**, 731–732.
RAMBALDI, E.R., RAJAN, R.S., WANG, D. and HOUSLEY, E.M. (1983): Evidence for relict grains in chondrules of Qingzhen, an E3 type enstatite chondrite. Earth Planet. Sci. Lett., **66**, 11–24.
RAMBALDI, E.R., HOUSLEY, R.M. and RAJAN, R.S. (1984): Occurrence of oxidized components in Qingzhen enstatite chondrite. Nature, **311**, 138–140.
WARK, D.A. and LOVERING, J.F. (1977): Marker events in the early evolution of the solar system; Evidence from rims on Ca-Al-rich inclusions in carbonaceous chondrites. Proc. Lunar Sci. Conf., 8th, 95–112.
WARK, D.A. and LOVERING, J.F. (1982a): The nature and origin of type B1 and B2 Ca-Al-rich inclusions in the Allende meteorite. Geochim. Cosmochim. Acta, **46**, 2581–2594.
WARK, D.A. and LOVERING, J.F. (1982b): Evolution of Ca-Al-rich bodies in the earliest solar system; Growth by incorporation. Geochim. Cosmochim. Acta, **46**, 2595–2607.

(Received October 5, 1987; Revised manuscript received December 1, 1987)

Appendix

Chemical compositions of the constituent minerals in unusual silicate-inclusions Nos. 172 (Columns 2–5), 167 (Columns 6–13), 152 (Columns 14–85), 300 (Columns 86–105), 303 (Columns 106–118), 302 (Columns 119–123), 114 (Columns 124–129), 237 (Columns 130–141), and 304 (Columns 142–143). En, Gm, Sp, Fas, Aug, SubAug, Di, Pig, Pl, Ab, dOl, Br, sEn, rimPx, and Ne are primary enstatite, groundmass, spinel, fassaite, augite, subcalcic augite, diopside, pigeonite, plagioclase, albite, decomposed-olivine, bronzite, secondary enstatite, rim pyroxene, and nepheline, respectively.

	1	2	3	4	5	6	7	8	9	10	11	12
1		172	172	172	172	167	167	167	167	167	167	167
2		Fas	Gm	Gm	Gm	En	En	Gm	Gm	Gm	Gm	Gm
3	SiO2	38.75	38.27	38.18	38.81	53.28	55.58	41.34	42.76	45.25	45.55	50.42
4	TiO2	0.75	0.39	0.87	0.56	0.32	0.44	0.09	0.00	0.07	0.00	0.41
5	Al203	26.91	31.05	24.03	30.26	3.22	3.09	2.79	4.61	16.54	18.67	7.59
6	Cr203	0.00	0.04	0.00	0.00	0.74	0.63	0.32	0.25	0.13	0.13	0.61
7	FeO	0.60	0.61	0.27	0.06	2.18	2.38	4.93	4.13	2.67	2.23	3.31
8	MnO	0.00	0.00	0.00	0.00	0.07	0.09	0.00	0.00	0.00	0.08	0.00
9	MgO	19.70	12.57	24.54	14.66	33.72	33.80	50.39	45.97	24.80	22.88	29.47
10	CaO	11.30	11.62	8.74	12.21	4.28	3.76	1.36	2.04	6.89	7.30	5.63
11	Na20	0.93	3.27	1.92	2.02	0.15	0.11	0.12	0.88	1.81	2.93	0.65
12	K20	0.08	0.71	0.38	0.14	0.00	0.00	0.00	0.11	0.06	0.21	0.03
13	Total	99.02	98.53	98.93	98.72	97.96	99.88	101.34	100.75	98.22	99.98	98.12

	13	14	15	16	17	18	19	20	21	22	23	24
1	167	152	152	152	152	152	152	152	152	152	152	152
2	Gm	Sp	Sp	Sp	Sp	Sp	Sp	Sp	Sp	Sp	Fas	Fas
3	51.56										46.22	45.54
4	0.54	0.38	0.30	0.41	0.35	0.36	0.34	0.60	0.10	0.35	1.20	1.16
5	3.92	45.77	48.70	48.61	49.92	47.35	48.29	48.90	49.69	48.56	12.35	12.92
6	0.83	27.64	24.37	25.58	23.74	25.58	25.73	25.45	24.27	23.69	0.61	0.84
7	2.35	0.37	0.41	0.43	0.44	0.47	0.55	0.87	1.99	2.24	4.24	4.32
8	0.09	0.00	0.00	0.00	0.00	0.21	0.05	0.00	0.09	0.00	0.00	0.00
9	31.91	24.51	25.22	25.16	24.96	25.32	24.45	24.73	23.41	24.74	13.45	13.09
10	7.48	0.08	0.06	0.06	0.06	0.13	0.11	0.15	0.37	0.48	22.66	21.86
11	0.07										0.06	0.11
12	0.00										0.00	0.02
13	98.75	98.75	99.06	100.25	99.47	99.42	99.52	100.70	99.92	100.06	100.79	99.86

	25	26	27	28	29	30	31	32	33	34	35	36
1	152	152	152	152	152	152	152	152	152	152	152	152
2	Fas	Fas	Fas	Fas	Fas	Fas	Fas	Aug	Aug	Aug	Aug	Aug
3	44.66	46.26	44.50	45.75	45.61	45.20	46.96	50.10	49.29	49.56	48.57	48.25
4	1.08	1.11	0.86	0.95	1.02	1.13	0.85	1.24	1.47	1.19	1.33	1.33
5	13.37	13.81	13.33	12.43	12.75	13.08	12.86	4.61	5.31	6.52	8.22	5.58
6	0.60	0.84	0.59	0.76	0.75	0.92	0.63	0.59	0.45	0.41	0.41	0.42
7	4.65	4.07	4.24	4.55	4.26	4.83	4.58	10.51	7.99	8.55	7.42	9.43
8	0.19	0.19	0.30	0.16	0.42	0.08	0.08	0.36	0.23	0.31	0.19	0.13
9	12.65	13.26	13.35	13.59	13.46	13.19	13.28	15.98	15.57	14.79	13.25	15.35
10	21.71	21.07	21.65	20.35	21.09	21.23	21.05	15.49	19.23	17.48	19.20	18.53
11	0.06	0.11	0.00	0.00	0.00	0.15	0.28	0.08	0.00	0.23	0.30	0.00
12	0.00	0.00	0.05	0.00	0.00	0.00	0.07	0.00	0.05	0.03	0.03	0.00
13	98.97	100.72	98.87	98.54	99.36	99.81	100.64	98.96	99.59	99.07	98.92	99.02

	37	38	39	40	41	42	43	44	45	46	47	48
1	152	152	152	152	152	152	152	152	152	152	152	152
2	Aug	Aug	Aug	Aug	Aug	Aug	Aug	Aug	Aug	Aug	Aug	Aug
3	48.24	49.13	49.12	49.27	50.48	49.95	49.26	48.33	50.12	48.52	51.00	50.87
4	1.62	1.40	1.46	1.25	1.30	1.56	1.36	1.68	1.43	1.63	1.25	1.20
5	5.13	5.08	4.45	5.63	4.66	4.42	5.29	6.27	4.81	5.43	2.88	4.59
6	0.41	0.55	0.33	0.59	0.78	0.88	0.54	0.81	0.59	0.40	0.46	0.40
7	8.62	8.64	9.83	7.56	8.87	8.33	8.65	7.12	8.36	8.97	11.92	9.70
8	0.25	0.40	0.19	0.23	0.16	0.32	0.39	0.16	0.43	0.22	0.36	0.29
9	14.89	13.99	15.49	15.14	15.54	16.37	16.04	14.03	15.54	14.61	17.90	17.38
10	19.44	19.21	18.18	20.59	19.44	19.05	18.40	20.64	17.97	18.53	12.35	15.63
11	0.04	0.19	0.05	0.10	0.04	0.06	0.00	0.00	0.06	0.05	0.11	0.12
12	0.04	0.00	0.00	0.00	0.02	0.00	0.00	0.00	0.05	0.05	0.00	0.02
13	98.68	98.59	99.10	100.36	101.29	100.94	99.93	99.04	99.36	98.41	98.23	100.20

	49	50	51	52	53	54	55	56	57	58	59	60
1	152	152	152	152	152	152	152	152	152	152	152	152
2	Aug	Aug	Aug	Aug	Aug	Aug	Aug	Aug	Aug	SubAug	SubAug	SubAug
3	50.25	47.74	47.93	49.51	50.18	49.68	49.61	48.90	49.77	51.47	50.94	52.09
4	1.06	1.47	1.39	1.35	1.31	1.04	1.39	1.42	1.07	1.00	0.94	0.82
5	3.63	5.82	6.25	4.24	3.22	5.21	5.46	5.15	3.93	2.91	2.90	2.70
6	0.35	0.60	0.61	0.47	0.45	0.58	0.49	0.47	0.20	0.21	0.28	0.30
7	8.44	9.32	8.38	10.56	11.73	9.21	7.33	8.29	11.17	11.29	11.57	13.23
8	0.23	0.25	0.19	0.29	0.46	0.10	0.34	0.23	0.21	0.42	0.44	0.31
9	15.24	14.58	13.96	17.04	18.11	15.74	15.86	15.20	16.78	20.97	19.72	21.46
10	19.50	19.40	19.98	15.75	13.08	17.97	18.17	18.82	15.12	11.51	11.95	8.31
11	0.17	0.16	0.00	0.00	0.14	0.00	0.10	0.10	0.08	0.03	0.17	0.07
12	0.05	0.00	0.00	0.00	0.00	0.00	0.00	0.00	0.03	0.00	0.00	0.00
13	98.92	99.34	98.69	99.21	98.68	99.53	98.75	98.58	98.36	99.81	98.91	99.29

	61	62	63	64	65	66	67	68	69	70	71	72
1	152	152	152	152	152	152	152	152	152	152	152	152
2	SubAug	SubAug	Pig	Pig	Pig	Pig	Pig	Pig	Pl	Pl	Pl	Pl
3	52.22	51.70	51.55	51.28	52.65	51.89	51.05	51.84	45.25	44.64	47.23	47.07
4	0.83	1.12	1.24	0.80	0.98	0.96	1.17	1.02	0.02	0.00	0.03	0.09
5	3.07	2.47	2.20	1.79	1.83	2.53	2.50	2.36	33.00	34.92	31.68	32.23
6	0.27	0.22	0.16	0.14	0.25	0.10	0.19	0.16	0.10	0.00	0.00	0.07
7	11.37	12.78	13.05	16.01	11.66	14.44	13.74	13.06	1.63	0.73	0.57	0.78
8	0.29	0.20	0.39	0.18	0.30	0.32	0.27	0.33	0.00	0.00	0.16	0.00
9	22.01	21.43	23.29	22.44	25.74	23.28	24.23	22.46	0.78	1.51	3.25	2.50
10	10.24	8.92	6.59	6.11	6.80	6.46	5.77	7.26	15.03	17.40	15.06	15.76
11	0.00	0.00	0.10	0.13	0.09	0.13	0.27	0.10	3.02	1.27	2.64	2.34
12	0.00	0.00	0.06	0.00	0.00	0.07	0.04	0.00	0.10	0.00	0.08	0.12
13	100.30	98.84	98.63	98.88	100.30	100.18	99.23	98.59	98.93	100.47	100.70	100.96

	73	74	75	76	77	78	79	80	81	82	83	84
1	152	152	152	152	152	152	152	152	152	152	152	152
2	Pl	Pl	Pl	Pl	Pl	Ab	Ab	dOl	dOl	dOl	dOl	dOl
3	49.62	44.76	46.86	43.34	46.14	71.43	71.85	36.72	36.95	36.25	37.96	40.95
4	0.17	0.00	0.13	0.00	0.00	0.00	0.07	0.12	0.06	0.00	0.12	0.12
5	30.88	34.60	31.42	33.97	32.09	17.23	17.00	1.99	0.35	0.09	0.20	0.14
6	0.00	0.00	0.00	0.04	0.12	0.03	0.82	0.17	0.59	0.16	0.21	0.31
7	0.84	0.37	1.12	0.80	0.75	0.83	0.74	13.27	13.74	13.53	14.12	10.20
8	0.00	0.00	0.00	0.00	0.00	0.00	0.00	0.00	0.25	0.35	0.13	0.19
9	2.34	1.43	2.47	2.10	2.60	0.23	0.32	46.63	46.91	48.48	46.14	47.06
10	13.01	17.30	14.71	15.06	15.17	0.17	0.27	1.32	0.96	0.25	0.86	0.57
11	3.86	1.29	2.56	3.53	2.33	8.88	8.50	0.21	0.15	0.03	0.16	0.28
12	0.20	0.05	0.00	0.25	0.10	0.73	0.58	0.01	0.00	0.03	0.02	0.03
13	100.92	99.80	99.27	99.09	99.30	99.53	100.15	100.44	99.96	99.17	99.92	99.85

	85	86	87	88	89	90	91	92	93	94	95	96
1	152	300	300	300	300	300	300	300	300	300	300	300
2	dOl	Br	Br	Br	Br	Br	Br	Br	Br	Br	sEn	sEn
3	37.00	56.78	56.43	56.37	55.58	55.62	55.98	55.74	55.54	55.35	58.71	58.43
4	0.11	0.00	0.00	0.10	0.02	0.00	0.13	0.12	0.10	0.03	0.00	0.00
5	0.16	0.47	0.37	0.35	0.39	0.45	0.75	0.56	0.48	0.49	0.09	0.06
6	0.24	0.75	0.78	1.04	0.78	0.82	0.98	0.77	0.80	0.82	0.03	0.07
7	14.79	8.36	7.24	8.48	9.30	7.42	9.34	9.63	9.54	9.25	0.48	0.54
8	0.15	0.14	0.29	0.22	0.15	0.17	0.37	0.11	0.00	0.18	0.00	0.00
9	46.14	33.48	34.04	33.11	32.12	34.50	32.30	33.01	32.66	32.55	41.41	39.33
10	0.36	0.65	0.60	0.30	0.57	0.59	0.68	0.64	0.65	0.67	0.12	0.06
11	0.07	0.00	0.08	0.04	0.00	0.18	0.06	0.00	0.00	0.00	0.05	0.00
12	0.02	0.00	0.04	0.00	0.03	0.05	0.00	0.00	0.03	0.00	0.03	0.00
13	99.04	100.63	99.87	100.01	98.94	99.80	100.59	100.58	99.80	99.34	100.92	98.49

	97	98	99	100	101	102	103	104	105	106	107	108
1	300	300	300	300	300	300	300	300	300	303	303	303
2	sEn	dOl	dOl	dOl	rimPx	rimPx	rimPx	rimPx	rimPx	Sp	Sp	Sp
3	59.18	37.46	39.22	38.27	54.63	56.85	55.01	56.35	55.66			
4	0.00	0.00	0.03	0.00	0.02	0.08	0.05	0.08	0.11	1.50	0.27	1.06
5	0.02	0.02	0.03	0.08	0.39	0.52	0.44	0.34	0.45	50.49	55.14	53.92
6	0.06	0.18	0.24	0.34	0.99	1.07	0.92	0.93	1.44	19.98	17.37	18.71
7	0.37	12.24	8.69	13.13	8.73	8.08	7.80	8.26	7.50	2.94	3.11	2.39
8	0.00	0.00	0.17	0.09	0.16	0.25	0.20	0.34	0.97	0.00	0.00	0.00
9	41.05	51.67	52.58	48.24	33.62	33.71	33.03	33.65	32.73	23.65	25.25	24.67
10	0.02	0.07	0.12	0.18	0.68	0.31	0.57	0.32	0.68	0.19	0.05	0.26
11	0.09	0.00	0.00	0.00	0.12	0.10	0.17	0.00	0.03			
12	0.00	0.00	0.02	0.00	0.00	0.00	0.02	0.00	0.06			
13	100.79	101.64	101.10	100.33	99.34	100.97	98.21	100.27	99.63	98.75	101.19	101.01

	109	110	111	112	113	114	115	116	117	118	119	120
1	303	303	303	303	303	303	303	303	303	303	302	302
2	Pl	Pl	Pl	sEn	sEn	sEn	dOl	dOl	Ne	Ab	Fas	Fas
3	44.85	44.57	49.37	58.82	58.21	58.86	33.04	33.56	44.21	71.92	43.46	43.86
4	0.00	0.11	0.00	0.00	0.00	0.00	0.38	0.18	0.00	0.04	1.35	1.35
5	33.94	35.61	32.23	0.08	0.12	0.06	0.32	0.15	35.06	15.74	13.20	13.41
6	0.00	0.01	0.02	0.00	0.00	0.00	0.40	0.48	0.04	0.00	1.03	0.63
7	0.79	0.47	1.12	0.42	0.36	0.38	15.47	15.47	1.25	0.45	3.87	3.83
8	0.00	0.00	0.00	0.00	0.00	0.00	0.41	0.00	0.11	0.00	0.45	0.00
9	1.72	0.92	0.18	41.00	40.80	40.70	48.02	47.99	0.55	1.35	13.61	14.53
10	16.78	17.10	14.27	0.03	0.11	0.00	2.88	2.38	1.28	0.54	21.54	21.40
11	2.60	2.39	3.42	0.05	0.04	0.00	0.55	0.17	18.57	8.61	0.14	0.00
12	0.07	0.02	0.17	0.03	0.00	0.00	0.05	0.00	0.11	0.98	0.00	0.10
13	100.75	101.20	100.78	100.43	99.64	100.00	101.52	100.38	101.18	99.63	98.65	99.11

	121	122	123	124	125	126	127	128	129	130	131	132
1	302	302	302	114	114	114	114	114	114	237	237	237
2	dOl	dOl	Gm	Br	Br	En	dOl	dOl	dOl	Di	Di	Pig
3	36.23	35.11	51.63	53.61	53.13	56.43	37.56	34.73	41.14	51.32	50.79	53.82
4	0.07	0.03	0.46	0.10	0.00	0.07	0.00	0.00	0.05	1.01	1.04	0.78
5	1.22	0.26	23.17	0.20	0.13	0.07	0.04	0.00	0.00	4.55	4.79	3.18
6	0.20	0.22	0.19	0.88	0.64	0.10	0.38	0.30	0.35	1.28	1.22	1.17
7	11.39	13.55	3.91	11.98	11.55	1.41	11.33	16.80	12.75	2.57	2.64	3.82
8	0.00	0.39	0.00	0.63	0.23	0.00	0.00	0.00	0.00	0.17	0.08	0.19
9	47.33	51.27	8.13	31.26	31.67	40.46	49.33	49.01	46.89	22.42	20.23	30.65
10	2.23	0.37	7.57	0.31	0.24	0.06	0.00	0.00	0.00	15.84	19.07	7.21
11	0.13	0.06	6.12	0.05	0.09	0.13	0.00	0.12	0.00	0.00	0.00	0.04
12	0.00	0.05	0.22	0.00	0.00	0.00	0.00	0.00	0.00	0.06	0.00	0.03
13	98.80	101.31	101.40	99.02	97.68	98.73	98.64	100.96	101.18	99.22	99.86	100.89

	133	134	135	136	137	138	139	140	141	142	143
1	237	237	237	237	237	237	237	237	237	304	304
2	Pig	Pig	Pl	Pl	dOl	dOl	dOl	dOl	dOl	Br	Br
3	52.58	52.98	45.77	46.91	39.77	39.80	38.47	38.80	39.44	55.41	55.72
4	0.77	1.00	0.05	0.09	0.00	0.00	0.00	0.00	0.05	0.00	0.02
5	3.07	3.15	32.13	31.62	0.03	0.04	0.00	0.10	0.00	0.00	0.00
6	1.14	1.00	0.10	0.07	0.60	0.50	0.42	0.54	0.44	0.75	0.81
7	4.52	4.57	0.89	0.47	4.79	5.39	4.83	5.38	4.96	9.56	9.66
8	0.12	0.06	0.00	0.09	0.15	0.06	0.00	0.28	0.00	0.10	0.07
9	31.29	31.10	3.22	2.18	54.85	55.12	54.85	54.81	54.35	34.68	33.88
10	5.29	5.64	12.76	14.93	0.30	0.33	0.29	0.32	0.27	0.13	0.07
11	0.00	0.00	4.10	2.64	0.00	0.00	0.00	0.00	0.00	0.06	0.00
12	0.00	0.00	0.27	0.12	0.05	0.00	0.00	0.00	0.00	0.03	0.04
13	98.78	99.50	99.29	99.12	100.54	101.24	98.86	100.23	99.51	100.72	100.27